JOURNAL OF GUIDANCE, CONTROL, AND DYNAMICS
Vol. 27, No. 2, March–April 2004

Precise Cassini Navigation During Solar Conjunctions Through Multifrequency Plasma Calibrations

P. Tortora*
University of Bologna, 47100 Forlì, Italy
L. Iess†
University of Rome "La Sapienza," 00184 Rome, Italy
and
J. J. Bordi,‡ J. E. Ekelund,§ and D. C. Roth¶
Jet Propulsion Laboratory, California Institute of Technology, Pasadena, California 91109

The Cassini spacecraft and its ground segment are currently testing a novel radio frequency multilink technology to perform radio science experiments. During solar conjunctions, this allows the complete removal of the solar plasma noise from the Doppler observables, with benefits for deep space navigation as well. This is obtained combining the carrier frequencies of three independent downlinks; two of them, at X and Ka band (Ka1), are coherent with an X-band uplink, whereas an additional Ka-band downlink (Ka2) is coherent with a Ka-band uplink. During the June–July 2002 Cassini solar conjunction, this procedure was fully tested for the first time. It is shown that, using the adopted multifrequency plasma calibration scheme, the standard deviation of the Doppler frequency residuals is reduced up to a factor of 200 over the uncalibrated X-band data. This large improvement in the data quality, revealed by values of the frequency stability previously achieved only during solar oppositions, makes the navigation accuracy of deep space probes nearly independent of the solar elongation angle.

Introduction

CURRENT deep space navigation systems rely on X-band radio links, used for both range and range-rate measurements. The frequency stability of these links (measured by the Allan deviation) is generally on the order of 10^{-13} at 1000 s integration time,[1] yielding range-rate accuracies on the order of 1.5×10^{-3} cm/s. Near solar oppositions, when the sun–Earth–probe (SEP) angle is close to 180 deg, higher stabilities (on the order of 2×10^{-14}) can be achieved because the solar wind velocity is nearly parallel to the line of sight.[2] For missions in the ecliptic plane, the largest instabilities are obtained during solar conjunctions (SEP angles close to zero) lasting up to two weeks. The dramatic decay in the attainable navigation accuracy is caused by the signal phase scintillation due to the solar plasma. Radiometric data collected when the line of sight falls within 40 solar radii from the sun are generally not used for the orbit determination process because of the high measurement errors introduced by the solar corona, which lead to long time spans during which navigation cannot rely on actual data.

More than 30 days of tracking data, across the 2000 and 2001 solar conjunctions, were removed for the orbit reconstruction of the Cassini spacecraft, currently in cruise flight to Saturn.[3–5] This strategy is widely accepted and proven during the cruise flight, but it is not recommended during critical mission phases, when frequent ground-commanded maneuvers are executed. An example of this is the Cassini Saturn orbit insertion (SOI) maneuver, scheduled on 1 July 2004, only seven days before a solar conjunction.[6] To reduce the orbit determination uncertainties, the whole maneuver would greatly benefit from using all radiometric data collected leading up to and following SOI.

The Cassini spacecraft and ground segment are currently used to test a novel multilink radio frequency system to perform radio science experiments (RSE). In addition to the standard X-band uplink/X-band downlink (X/X), the onboard configuration provides an exciter KEX, which generates a Ka-band downlink signal (at 32.5 GHz), coherent with the received X-band uplink, resulting in an X/Ka link. Moreover, a Ka/Ka link is obtained using a coherent frequency translator (KaT), which transmits to the ground a Ka-band signal (at 32.5 GHz) coherent with a Ka-band uplink (at 34 GHz). The primary goals of RSE are the measurement of the solar gravitational deflection during the Solar conjunction experiments (SCE)[7,8] and the search for low-frequency gravitational waves (due, for example, to the coalescence of massive black hole binaries) during solar oppositions.[9]

Originally proposed to calibrate the Doppler observables used for the estimation of the post-Newtonian parameter γ during the SCE, the multifrequency plasma calibration scheme[10] has also shown to be very effective in improving the accuracy of the orbit determination process. This has been demonstrated during the test of the Cassini ground and onboard systems, performed on May–June 2001 (Ref. 11) and during the June–July 2002 solar conjunction.[12] With this method, the sky frequencies, which are reconstructed using data from a wideband open-loop receiver (OL) in the three bands (X/X, X/Ka, and Ka/Ka), are coherently combined to remove the effects of the solar plasma, the major noise source in the Doppler observable. However, the observables used by the orbit determination program (ODP) developed at the Jet Propulsion Laboratory are obtained from the block V receivers, which digitally lock and track the carrier in a closed loop. Thus, using the OL plasma calibrated sky frequencies for the orbit determination process requires the additional computation of Doppler observables compatible with the data format required by the ODP.

The analysis of the 2001 Cassini solar conjunction data[11] has shown that the use of the multifrequency plasma calibration scheme

Presented as Paper 2003-200 at the AAS/AIAA 13th Space Flight Mechanics Meeting, Ponce, Puerto Rico, USA, 9–13 February 2003; received 31 March 2003; revision received 6 June 2003; accepted for publication 11 June 2003.

*Assistant Professor, II Facoltà di Ingegneria, Via Fontanelle 40; paolo.tortora@unibo.it. Member AIAA.
†Associate Professor, Dipartimento di Ingegneria Aerospaziale ed Astronautica, Via Eudossiana 18; iess@hermes.ing.uniroma1.it. Member AIAA.
‡Member Technical Staff, Navigation and Mission Design Section, 4800 Oak Grove Drive; John.J.Bordi@jpl.nasa.gov.
§Member Technical Staff, Navigation and Mission Design Section, 4800 Oak Grove Drive; John.E.Ekelund@jpl.nasa.gov.
¶Member Technical Staff, Navigation and Mission Design Section, 4800 Oak Grove Drive; Duane.C.Roth@jpl.nasa.gov.

can lower the Allan deviation to values of 2×10^{-14}, at integration times of 1000 s, when the relative distance of the line-of-sight vector from the center of the sun (impact parameter) is about 25 solar radii. This corresponds to a range-rate accuracy of about 3×10^{-4} cm/s. At an impact parameter of about 6 solar radii, the Allan deviation is on the order of 4×10^{-14} (1000 s integration time), still well below the corresponding original uncalibrated X-band value and a factor of 25 better than the Ka-band value.

For the 2002 Cassini solar conjunction, a much wider data set has been analyzed.[12] The results show that, although the stability of the uncalibrated links degrades as the line of sight gets closer to the sun, the Allan deviation of the plasma calibrated frequency residuals has nearly constant values of $1–2 \times 10^{-14}$ at integration times of 1000 s. Similar values were previously achieved only near solar oppositions.

In addition to the plasma calibrations, at the Deep Space Station (DSS) 25, part of the Deep Space Network (DSN) complex in Goldstone, California, an advanced media calibration (AMC) system has been developed and implemented to perform RSE. It consists of water vapor radiometers, digital pressure sensors, and microwave temperature profilers[13,14] providing a precise calibration of the frequency shifts due to the dry and wet components of the Earth troposphere. The analysis of the calibration data collected during the 2002 Cassini solar conjunction has shown that the frequency stability is improved by about a factor of three, when the AMC is applied to the navigation data rather than the standard seasonal tropospheric models.

The remainder of this paper is organized as follows: First a brief description of the June–July 2002 Cassini solar conjunction is given, pointing out the geometry of the Cassini trajectory as seen from the Earth and summarizing the data acquired. The algorithm to reconstruct the sky frequencies from wideband OL data is then illustrated, followed by a description of the solar effects on signal properties. The plasma calibration scheme, used to generate the plasma-free observables, is described and, using a simple model of the orbital dynamics, the stability of the residuals is characterized in terms of Allan deviations. In the following section, the techniques for the reduction of the nondispersive tropospheric effects are analyzed, using the advanced media calibration system. We then compare the frequency residuals and orbital solutions obtained using uncalibrated and calibrated data in the ODP. Finally, concluding remarks are given in the last section.

Geometry of the 2002 Cassini Solar Conjunction

During the June–July 2002 Cassini first SCE (SCE1), the radio science instrumentation onboard the spacecraft and at the DSN ground stations was operated continuously. At the DSS 25 antenna, the only one with Ka-band uplink capability, the OL receivers acquired and sampled the downlink carrier in three bands (X/X, X/Ka, and Ka/Ka), whereas at the DSS 45 (Canberra, Australia) and DSS 65 (Madrid, Spain) the OL receivers acquired only the X/X signal. Table 1 shows a summary of both the expected and actually acquired data for the days of year (DOY) 157/2002–186/2002 (from 6 June to 5 July 2002). The amount of data acquired for the X/Ka link at DSS 25 is identical to that of the X/X link.

The relatively low percentage of Ka/Ka data acquired at DSS 25 was due to a malfunctioning of the Ka-band uplink transmitter, caused by a heat exchanger problem. This resulted in either the complete absence of data for some passes or some tracks being shorter than expected.

Table 1 Summary of OL data acquired at DSN stations during the 2002 Cassini solar conjunction

Band	DSN station	Cumulative expected pass duration, h/min	Cumulative actual pass duration, h/min	% Acquired
X/X	DSS 25	359/00	340.08	95
Ka/Ka	DSS 25	262/40	188.15	72
X/X	DSS 45	129/20	125.08	97
X/X	DSS 65	254/36	241.21	95

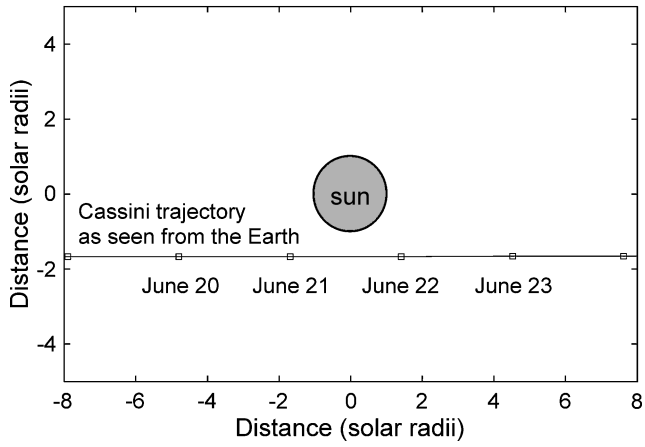

Fig. 1 Cassini trajectory with respect to the sun during the 2002 solar conjunction.

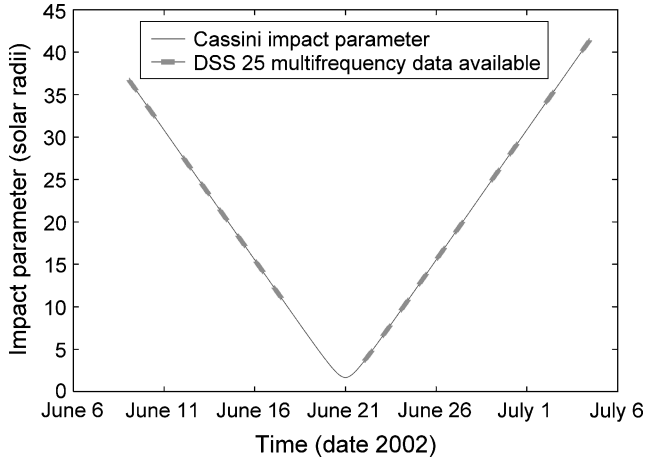

Fig. 2 Cassini sun impact parameter vs time during the 2002 solar conjunction.

The plasma calibration is made possible by the simultaneous acquisition of the down-link signals in the three bands. The amount of multifrequency data expected and actually acquired at DSS 25 is summarized as follows: the cumulative expected pass duration was 262 h and 40 min and the cumulative actual pass duration was 166 h and 35 min, which is 63% acquired. In practice this represents the overlap between the X/X and Ka/Ka data sets. For the preceding data, actual tracks shorter than 5 h were not considered, and DOY 172 was discarded due to the inability to reliably estimate the X/X and X/Ka sky frequencies.

The geometry of the 2002 Cassini solar conjunction and the spacecraft impact parameter are shown in Figs. 1 and 2, respectively. The minimum SEP angle was reached on DOY 172/2002 (21 June) at about 1314 hrs, when the impact parameter was 1.6 solar radii. The multifrequency link data closest to conjunction were acquired on 22 June, at an impact parameter of about 3.5 solar radii.

Reconstruction and Characterization of the OL Sky Frequencies

During conjunctions, the radio waves received at the ground station are corrupted by the solar and interplanetary plasma. This noise is inherently nonstationary, and its effects are strongly correlated among the three bands. The refractive index of the plasma differs from unity by a quantity proportional to the inverse square of the carrier frequency; thus, Ka-band signals are much less perturbed by the corona than X-band signals. However, even a Ka-band carrier shows strong scintillation when the beam is very close to the sun (less than about 5 solar radii). In the radio science receivers (RSR), the carrier is downconverted to nearly zero frequency using an accurate model of the signal dynamics and then sampled at the

preselected rate (1 kHz in our case). To allow for a full reconstruction, a complex representation is used, where the incoming carrier is beaten against two 90-deg phase-shifted reference signals.

The RSR files, acquired at the DSN complexes, consist of records of the in-phase (I) and in-quadrature (Q) components of the down-converted carrier, plus a header containing ancillary information needed for a full reconstruction of the signal.

The procedure for the reconstruction of the sky frequency from OL data acquired at solar conjunction has been described in Ref. 11. It has been shown that the typical algorithms used to reconstruct the signal frequency from digital samples, involving a digital phase-locked loop implemented on a computer, are not suitable at impact parameters below 6–8 solar radii. The strong phase scintillation causes frequent loss of lock, especially for the X/X and X/Ka carriers, which leads to a significant loss of data.

A different frequency reconstruction algorithm, consisting of a frequency estimator that processes sequentially (and independently) fixed-length data intervals, was implemented for the Cassini conjunction experiment.

The X/X, X/Ka, and Ka/Ka observables have also been characterized by analyzing their frequency residuals.[12] To this end, the sky frequencies have been fitted using a simple orbital model,[11] which is based on the assumption that the signal dynamics over timescales of a few hours (a tracking pass) is affected only by the Earth rotation and linear drifts of the spacecraft angular coordinates (right ascension and declination) and radial velocity. When approaching and leaving conjunction, the stability of the three links is significantly degraded. In such conditions, the solar plasma noise affecting the radiometric data causes a dramatic decay in the attainable accuracy of the orbit solution. In Ref. 15, a method has been recently proposed to calibrate radiometric data collected during a solar conjunction. However, this method is not applicable to our case because it makes use of a combination of Doppler and ranging to estimate corrections to the navigation observables. Thus, for interplanetary missions in the ecliptic plane, even if tracking can be performed a very short distance from the sun, when the impact parameter is lower than 40 solar radii, the quality of Doppler and ranging observables is so poor that these data are usually discarded in the orbit determination process. For the Cassini orbit reconstruction, about 30 days of radiometric data were removed across the 2000 and 2001 solar conjunctions.[5]

Computation of Plasma-Free Doppler Observables Using the Multifrequency Link

The output of the sky frequency reconstruction algorithm, summarized in the preceding section, is a set of three independent observables at each time instant,

$$(f_{\mathrm{sky}})^{\mathrm{obs}}_{\mathrm{X/X}}, \qquad (f_{\mathrm{sky}})^{\mathrm{obs}}_{\mathrm{X/Ka}}, \qquad (f_{\mathrm{sky}})^{\mathrm{obs}}_{\mathrm{Ka/Ka}} \tag{1}$$

where the subscript specifies the uplink and downlink band and the superscript identifies that they are observed quantities.

With the assumption that each observed sky frequency contains three independent contributions, due to the spacecraft orbital motion and to the crossing of the solar corona in the uplink and in the downlink, we define y as the relative frequency shift and write the following set of equations[10]:

$$\begin{aligned} y^{\mathrm{obs}}_{\mathrm{X/X}} &= y_{\mathrm{nd}} + y_{\mathrm{pl\_up}} + \left(1/\alpha^2_{\mathrm{X/X}}\right) y_{\mathrm{pl\_dn}} \\ y^{\mathrm{obs}}_{\mathrm{X/Ka}} &= y_{\mathrm{nd}} + y_{\mathrm{pl\_up}} + \left(1/\alpha^2_{\mathrm{X/Ka}}\right) y_{\mathrm{pl\_dn}} \\ y^{\mathrm{obs}}_{\mathrm{Ka/Ka}} &= y_{\mathrm{nd}} + (1/\beta^2) y_{\mathrm{pl\_up}} + (1/\beta^2)\left(1/\alpha^2_{\mathrm{Ka/Ka}}\right) \mathrm{y}_{\mathrm{pl\_dn}} \end{aligned} \tag{2}$$

where the turnaround ratios for the three links are $\alpha_{\mathrm{X/X}} = 880/749$, $\alpha_{\mathrm{X/Ka}} = 3344/749$, and $\alpha_{\mathrm{Ka/Ka}} = 14/15$ and $\beta = (f_{\mathrm{Ka}})_{\uparrow}/(f_{\mathrm{X}})_{\uparrow}$ is the ratio between the X- and Ka-band uplink frequencies. In Eq. (2), y_{nd} is the orbital (nondispersive) contribution, whereas $y_{\mathrm{pl\_up}}$ and $y_{\mathrm{pl\_dn}}$ are the plasma uplink and plasma downlink contributions to the relative frequency shift, respectively [referred to a $(f_{\mathrm{X}})_{\uparrow}$ carrier]. The observable frequency shifts as a function of the observed sky frequencies are

$$y^{\mathrm{obs}}_{\mathrm{X/X}} = \frac{(f_{\mathrm{sky}})^{\mathrm{obs}}_{\mathrm{X/X}}}{\alpha_{\mathrm{X/X}}(f_{\mathrm{X}})_{\uparrow}} - 1 \tag{3a}$$

$$y^{\mathrm{obs}}_{\mathrm{X/Ka}} = \frac{(f_{\mathrm{sky}})^{\mathrm{obs}}_{\mathrm{X/Ka}}}{\alpha_{\mathrm{X/Ka}}(f_{\mathrm{X}})_{\uparrow}} - 1 \tag{3b}$$

$$y^{\mathrm{obs}}_{\mathrm{Ka/Ka}} = \frac{(f_{\mathrm{sky}})^{\mathrm{obs}}_{\mathrm{Ka/Ka}}}{\alpha_{\mathrm{Ka/Ka}}(f_{\mathrm{Ka}})_{\uparrow}} - 1 \tag{3c}$$

The set of Eqs. (2) is easily solved for y_{nd}, $y_{\mathrm{pl\_up}}$, and $y_{\mathrm{pl\_dn}}$:

$$y_{\mathrm{pl\_dn}} = \left(\frac{1}{\alpha^2_{\mathrm{X/X}}} - \frac{1}{\alpha^2_{\mathrm{X/Ka}}}\right)^{-1} \left(y^{\mathrm{obs}}_{\mathrm{X/X}} - y^{\mathrm{obs}}_{\mathrm{X/Ka}}\right) \tag{4}$$

$$y_{\mathrm{pl\_up}} = \frac{y^{\mathrm{obs}}_{\mathrm{X/Ka}} - y^{\mathrm{obs}}_{\mathrm{Ka/Ka}} - y_{\mathrm{pl\_dn}}\left[1/\alpha^2_{\mathrm{X/Ka}} - (1/\beta^2)\left(1/\alpha^2_{\mathrm{Ka/Ka}}\right)\right]}{1 - 1/\beta^2} \tag{5}$$

$$y_{\mathrm{nd}} = y^{\mathrm{obs}}_{\mathrm{Ka/Ka}} - \left(y_{\mathrm{pl\_up}} + \frac{1}{\alpha^2_{\mathrm{Ka/Ka}}} y_{\mathrm{pl\_dn}}\right) \frac{1}{\beta^2} \tag{6}$$

Once the nondispersive relative frequency shift y_{nd} is solved for, one can compute the nondispersive sky frequency for each band. Therefore, for example, the nondispersive sky frequency for the X/X band can be written as

$$(f_{\mathrm{sky}})^{\mathrm{nd}}_{\mathrm{X/X}} = (f_{\mathrm{sky}})^{\mathrm{obs}}_{\mathrm{X/X}} - \alpha_{\mathrm{X/X}}(\Delta f_{\mathrm{X}})^{\mathrm{pl\_up}} - (\Delta f_{\mathrm{X}})^{\mathrm{pl\_dn}}/\alpha_{\mathrm{X/X}} \tag{7}$$

where $(\Delta f_{\mathrm{X}})^{\mathrm{pl\_up}} = y_{\mathrm{pl\_up}}(f_{\mathrm{X}})_{\uparrow}$ and $(\Delta f_{\mathrm{X}})^{\mathrm{pl\_dn}} = y_{\mathrm{pl\_dn}}(f_{\mathrm{X}})_{\uparrow}$.

Substituting in Eq. (7) and dividing by $\alpha_{\mathrm{X/X}}(f_{\mathrm{X}})_{\uparrow}$, we get

$$\frac{(f_{\mathrm{sky}})^{\mathrm{obs}}_{\mathrm{X/X}}}{\alpha_{\mathrm{X/X}}(f_{\mathrm{X}})_{\uparrow}} = \frac{(f_{\mathrm{sky}})^{\mathrm{nd}}_{\mathrm{X/X}}}{\alpha_{\mathrm{X/X}}(f_{\mathrm{X}})_{\uparrow}} + y_{\mathrm{pl\_up}} + \frac{y_{\mathrm{pl\_dn}}}{\alpha^2_{\mathrm{X/X}}}$$

which provides by the comparison with the first row of the set of Eqs. (2) and the use of Eq. (3) the result

$$(f_{\mathrm{sky}})^{\mathrm{nd}}_{\mathrm{X/X}} = (1 + y_{\mathrm{nd}})\alpha_{\mathrm{X/X}}(f_{\mathrm{X}})_{\uparrow} \tag{8}$$

Equation (8) shows that the so-called plasma-free (nondispersive) sky frequency (X/X band) is obtained as a linear combination of the three X/X, X/Ka, and Ka/Ka observables because, as shown in Eq. (6), they all contribute to the nondispersive frequency shift y_{nd}. The stability of the plasma-free link can be compared to the corresponding uncalibrated links by computing the Allan deviation of the frequency residuals obtained by fitting the sky frequency with the simple orbital model described in the preceding section.

Figure 3 shows a cumulative plot of the Allan deviations (at 1000 s integration time) for the available multifrequency link passes. For each pass, the stability of the raw X/X, X/Ka, and Ka/Ka links are directly compared to the corresponding plasma-free one. To avoid excessive contamination from tropospheric noise and systematic errors, only data acquired above 20 deg of elevation were considered.

Whereas the Allan deviation of the X/X, X/Ka, and Ka/Ka links degrades with smaller SEP angles, the plasma-free signal exhibits a nearly constant stability at levels of $1–2 \times 10^{-14}$, at integration times of 1000 s, a value previously achieved only near solar oppositions. The largest improvement in the signal stability is obtained on 24 June (DOY 175/2002), where the Allan deviation of the uncalibrated X/X signal is reduced by about three orders of magnitude. However, on 22 June, the plasma-free signal stability is about 50 times worse than its average value. This can be explained by considering that three main effects limit the applicability of the plasma calibration scheme [Eq. (2)] based on multifrequency links: 1) diffraction and physical optics effects, 2) magnetic corrections to the refractive index, and 3) spatial separation between the ray paths at different frequencies.

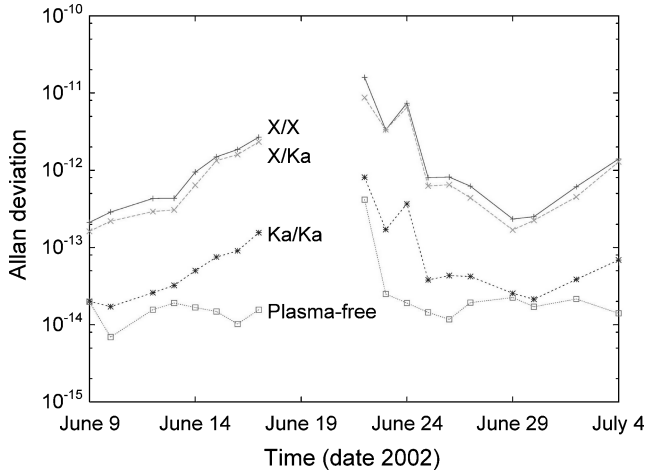

Fig. 3 Cassini Allan deviations at 1000 s integration time during the 2002 solar conjunction.

In Ref. 11, it was explained that at small impact parameters the diffraction effects due to physical optics are responsible for occasional signal fading at small SEP angles. Moreover, when the impact parameter is smaller than 5 solar radii [as it was on 22 June (Fig. 2)] both magnetic corrections to the refractive index and density gradients in the solar corona (which cause a change in the impact parameter) become nonnegligible.

In conclusion, Fig. 3 shows that, for the 30 days of the SCE1, the quality of the plasma calibrated Doppler observables is nearly independent of the SEP angle, with the exception of the pass on 22 June, where the impact parameter of the signal beam was smaller than 5 solar radii.

Advanced Media Calibration System

To perform the RSE, the DSS 25 complex has been equipped with an outstanding media calibration system[13,14] capable of providing a full calibration of the dry and wet path delays due to the Earth troposphere. It consists of two independent systems, where water vapor radiometers, digital pressure sensors, and microwave temperature profilers have been installed and located a short distance from the main 34-m antenna at the Goldstone, California, complex. This system was tested for the first time during the first gravitational wave experiment (GWE1), November 2001–January 2002 (Ref. 9).

In Ref. 8, the data reduction of the AMC acquired during the SCE1 has been described in detail. It has been shown that, for many tracking passes, the dry component of the zenith path delay was much noisier than the corresponding data acquired during the GWE1. It turned out with high probability that the larger zenith path delay fluctuations levels were due to the surface wind speed, which during many passes of the SCE1 exceeded 25–30 km/h. The increased zenith path delay noise levels then should be due to the atmosphere and not some wind-induced jiggle in the pressure sensor mechanism. An easy way to filter out the high-frequency dry zenith path delay fluctuations is to average the raw data acquired by the instruments, through a moving window (a 100-s interval used for the SCE1), to remove the local, small-scale effects.

The parallel analysis of the GWE1 and SCE1 advanced media calibrations data has revealed that the use of the water vapor radiometers and digital pressure sensors is more effective during solar conjunctions. This is mainly due to two concurrent reasons: First, SCEs are carried out during daytime, whereas GWEs take place during the night. Second, because of Cassini's present orbital position, for the northern hemisphere ground stations, the SCE observations are made in summer, whereas the GWE ones are in winter. As a result, the tropospheric noise levels, which can be reduced making use of the AMC, are significantly higher during SCE than GWE. As shown in the next section, the frequency stability is improved by about a factor of three, when the AMC, rather than the standard seasonal tropospheric models, is applied to the SCE1 navigation data.

Cassini Orbit Determination Using Plasma and Troposphere Calibrated Navigation Observables

In an earlier section, we pointed out the procedures needed to compute a plasma-free sky frequency using three independent signals simultaneously acquired in the bands X/X, X/Ka, and Ka/Ka. These calibrated sky frequencies can now be used to form a plasma-free Doppler observable compatible with the data format handled by the ODP.

For two-way Doppler observables, the ODP uses the received sky frequency in the following manner to compute the observable[16]:

$$\text{observable} = \alpha_{\text{up/dn}} \cdot f_{\text{ref}} - f_{\text{sky}} \tag{9}$$

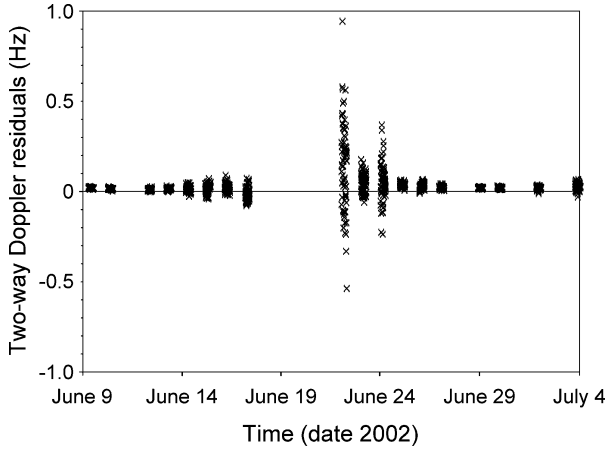

Fig. 4 Cassini X/X Doppler residuals without plasma calibrations and with standard troposphere calibrations.

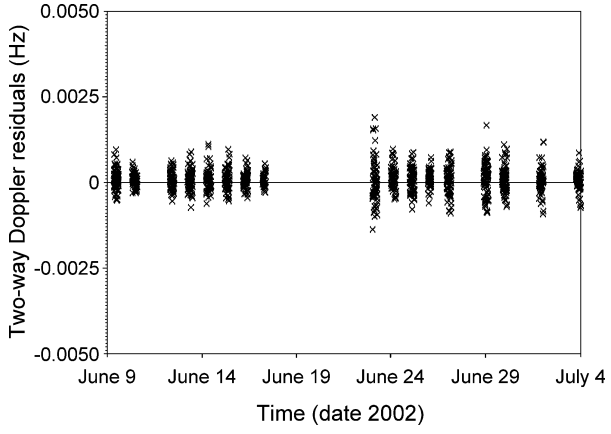

Fig. 5 Cassini X/X Doppler residuals including plasma calibrations and the standard troposphere calibrations.

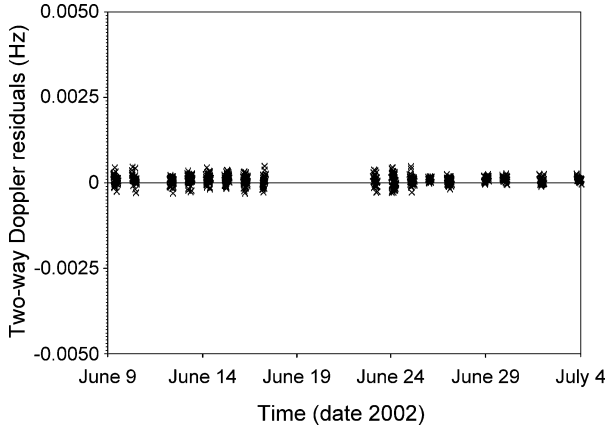

Fig. 6 Cassini X/X Doppler residuals including plasma calibrations and the advanced media calibrations.

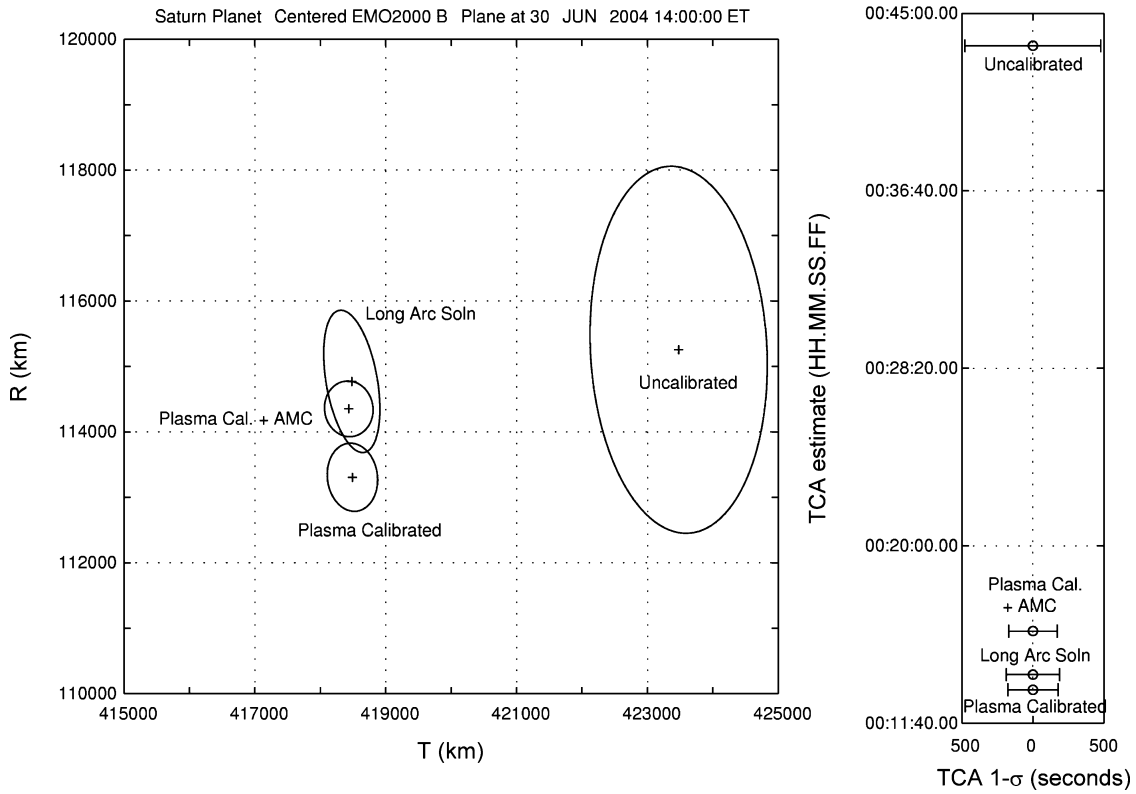

Fig. 7 Saturn-centered B plane of several Cassini orbital solutions obtained using different data sets.

where f_{ref} is the Doppler reference frequency and $\alpha_{\text{up/dn}}$ is the turnaround ratio, which depends only upon the downlink band because it is always referred to an S-band uplink carrier. [Note that one-way, two-way, and three-way Doppler observables are formed when 1) the spacecraft (S/C) generates a signal that is received at the ground station, 2) a ground station generates the uplink signal to the S/C and receives the downlink signal from it, and 3) the uplink signal to the S/C is generated in a ground station but the downlink signal from the S/C is received by a different ground station, respectively.] For an X-band downlink signal, $\alpha_{\text{S/X}} = 880/221$. Thus, at each timetag, the plasma calibrated sky frequency can be directly substituted to the corresponding uncalibrated one to form a plasma calibrated observable:

$$(\text{observable})^{\text{nd}}_{\text{X/X}} = \alpha_{\text{S/X}} \cdot f_{\text{ref}} - (f_{\text{sky}})^{\text{nd}}_{\text{X/X}} \tag{10}$$

The result of this procedure is a new navigation file where the Doppler observables, to be processed by the ODP, are free from solar plasma noise. This new observable has been computed using OL data (RSR files and a digital frequency estimator), which have been processed for the first time for orbit determination.

For a full comparison between the plasma-free and raw observables, we processed (in the ODP) the original, plasma free, and plasma free with the AMC navigation files, where the observables are compressed at 300 s.

To compare the results of using the three different tracking data sets in terms of spacecraft navigation, a short arc was processed, which spanned just the solar conjunction period (between 9 June and 5 July 2002). The initial conditions on 9 June 2002 were obtained from a long arc solution that has an epoch of 28 February 2001. The only parameters estimated in the short arc solutions were the S/C state and the radioisotope thermoelectric generator (RTG) radiation accelerations. For all three cases, only station DSS 25 two-way Doppler data were used. The weights assigned to the tracking data were assigned on a pass-by-pass basis, where the a priori uncertainty assigned to each pass is equal to the 1-σ value of the frequency residuals.

Figure 4 shows the two-way Doppler postfit residuals obtained by running the ODP and using the original (uncalibrated), X-band tracking data file.

Note the increasing variation of the frequency residuals when the S/C gets close to conjunction (which occurred on 21 June). On 24 June 2002, when the average level of the residuals was already returning to lower values, there is an evident signature in the data. This was already noticed in terms of increased Allan deviations in Fig. 3. That was probably caused by some large coronal mass ejections observed by the Solar and Heliospheric Observatory (SOHO)** in the region traversed by the Earth-to-Cassini line of sight. The overall 1-σ value of these residuals is 7.16×10^{-2} Hz.

Figure 5 shows exactly the same time interval of Fig. 4, but now including the plasma calibrated two-way Doppler residuals. The y-axis scale reveals that the noise reduction is huge with nearly constant levels for the 17 passes shown. The 22 June 2002 pass is not shown in the plot because it is the only one where the multifrequency plasma calibration scheme did not offer reliable results (Fig. 3). The 1-σ value of the plasma calibrated postfit residuals is 3.5×10^{-4} Hz, more than 200 times better than the corresponding uncalibrated ones.

Figure 6 shows the additional improvement in the stability of the frequency residuals, which can be obtained once the AMC is applied to the plasma calibrated navigation observables. For some passes, especially after conjunction, the noise reduction is close to a factor of five, whereas for some others the effectiveness of the advanced troposphere calibration is less evident. The 1-σ value of the plasma and media calibrated postfit residuals is 1.2×10^{-4} Hz a factor of 3 and 600, respectively, better than the corresponding plasma calibrated and uncalibrated ones.

To help visualize the differences in the solutions and the uncertainties in the estimates, the results are mapped forward to the Saturn B plane (perpendicular to the incoming asymptote at the target planet) in Fig. 7. For reference, the long arc solution and error ellipse is also shown in Fig. 7. The long arc solution is considered

**Data available on the SOHO home page online at URL: http://sohowww.nascom.nasa.gov [cited 24 May 2003].

Table 2 Summary of the RTG acceleration estimates obtained using different sets of X-band data and ODP setup

Case	RTG acceleration, km/s^2	1-σ Uncertainty, km/s^2
Long arc solution	-2.98×10^{-12}	0.05×10^{-12}
Uncalibrated short arc	-7.44×10^{-12}	1.12×10^{-12}
Plasma calibrated short arc	-2.89×10^{-12}	0.13×10^{-12}
Plasma calibrated plus AMC short arc	-3.07×10^{-12}	0.08×10^{-12}

the best estimate as of July 2002 of the Saturn B-plane location, and so it provides a measure of the accuracy of the short arc solutions. The uncalibrated solution is clearly the poorest, with a large offset in the B-plane T direction (Fig. 7) relative to the long arc solution. The solution made with the plasma calibrated data shows a significant improvement in the level of agreement with the long arc solution. Furthermore, the addition of the advanced media calibrations results in even better agreement with the long arc solution.

These results are impressive when considering that the short arc solutions rely on roughly 30 days of Doppler data from only one ground station during a solar conjunction. Note that the error ellipses and associated mean values in Fig. 7 are for comparison purpose only and do not represent current best knowledge of Cassini's ephemeris. In all cases, no attempt was made to model the errors associated with future maneuvers or thrusting events, which would normally dominate the size of the error ellipse. Furthermore, the actual mean values will differ because future spacecraft maneuvers and orientation changes that will impact the direction of the radiation accelerations are not modeled.

Another way to assess the quality of the solutions is to compare the value of the RTG acceleration estimate in the spacecraft z direction. A very accurate estimate of this value was made during the GWE1. The RTG acceleration estimate is very precise because during the GWE the spacecraft orientation was not changed and was maintained using the reaction wheels rather than the reaction control thrusters. Additionally, continuous 24-h tracking of the spacecraft was available during the GWE. The z direction of the RTG acceleration was well determined because the spacecraft was oriented such that the z axis was pointed toward Earth. Table 2 shows the values of the estimates of this parameter for the three different short arc cases, as well as the estimate from the long arc solution. Once again, the results show a dramatic improvement in comparison to the long arc solution when the solar plasma calibrations are included in the Doppler data. However, little improvement is seen in this parameter when the AMCs are included in the tracking data.

Conclusions

The Cassini spacecraft and its ground segment are equipped with an advanced radio frequency system to perform radio science experiments. In addition to the standard X-band downlink, coherent with an X-band uplink, the S/C onboard configuration allows two additional downlinks in the Ka band, one coherent with the X-band uplink and the other coherent with a Ka-band uplink. The simultaneous acquisition of the three downlink carriers is possible only at DSS 25, which is the only DSN station with a Ka-band uplink and downlink capability. This configuration, originally devised to perform an accurate test of the general relativity during solar conjunctions, allows the complete removal of the solar plasma noise from the Doppler observables. Moreover, DSS 25 has been equipped with an AMC system, which allows the full calibration of the dry and wet path delay components of the Earth troposphere.

During the 2002 Cassini solar conjunction experiment, the radio frequency system was operated continuously for 30 days, from 6 June through 5 July. The multifrequency plasma calibration scheme has been applied to all of those DSS 25 passes where the three independent downlinks were available (18 passes in total). Then, the plasma-free Doppler observables, derived from radio science OL receivers, have been fitted using the ODP to test the capabilities of the new system for precision S/C navigation. In addition, the advanced troposphere calibrations have been applied to the plasma calibrated data, resulting in a data set of the highest quality. The analysis of the ODP frequency residuals reveals that the application of the plasma and troposphere calibrations to the Doppler observables yields a global improvement of a factor of 600 over the corresponding uncalibrated data. Thus, with this new technique, the data acquired near solar conjunctions can be successfully calibrated to gain frequency stabilities and orbital solution accuracies usually recorded when the S/C is at solar oppositions.

During the 2003 Cassini second SCE, a real-time test of the plasma calibration technique adopted in this paper will be performed. The 30 days of continuous multifrequency tracking from DSS 25 will have the main goal of a second precise test of general relativity, but will also allow to gain further confidence in the capabilities of this novel method for S/C navigation. This experience is valuable in view of the potential applications for the SOI maneuver, which occurs only seven days before a solar conjunction, on 1 July 2004, and during the four solar conjunctions, which will occur during the Cassini Saturn tour (2004–2008).

Acknowledgments

The work of P. Tortora and L. Iess has been funded by the Italian Space Agency. The work of J. J. Bordi, J. E. Ekelund, and D. C. Roth was performed at the Jet Propulsion Laboratory, California Institute of Technology, under a contract with the National Aeronautics and Space Administration and was provided through the courtesy of NASA/JPL/Caltech, Pasadena, California.

References

[1]Thornton, C. L., and Border, J. S., "Range and Doppler Tracking Observables," *Radiometric Tracking Techniques for Deep-Space Navigation*, Deep-Space Communications and Navigation Series, Jet Propulsion Lab., JPL Publ. 00-11, California Inst. of Technology, Pasadena, CA, Oct. 2000, pp. 15–18.

[2]Armstrong, J. W., Woo, R., and Estabrook, F. B., "Interplanetary Phase Scintillation and the Search for Very Low Frequency Gravitational Radiation," *Astrophysical Journal*, Vol. 230, June 1979, pp. 570–574.

[3]Roth, D. C., Guman, M. D., Ionasescu, R., and Taylor, A. H., "Cassini Orbit Determination From Launch to the First Venus Flyby," AIAA Paper 98-4563, Aug. 1998.

[4]Guman, M. D., Roth, D. C., Ionasescu, R., Goodson, T. D., Taylor, A. H., and Jones, J. B., "Cassini Orbit Determination From First Venus Flyby to Earth Flyby," *Advances in the Astronautical Sciences, Spaceflight Mechanics 2000*, Vol. 105, Jan. 2000, pp. 1053–1072.

[5]Roth, D. C., Guman, M. D., and Ionasescu, R., "Cassini Orbit Reconstruction from Earth to Jupiter," *Advances in the Astronautical Sciences, Spaceflight Mechanics 2002*, Vol. 112, Jan. 2002, pp. 693–704.

[6]Cassini Mission Plan, rev. N, Jet Propulsion Lab., Rept. JPL D-5564, California Inst. of Technology, Pasadena, CA, May 2002.

[7]Iess, L., Giampieri, G., Anderson, J. D., and Bertotti, B., "Doppler Measurement of the Solar Gravitational Deflection," *Classical and Quantum Gravity*, Vol. 16, No. 5, 1999, pp. 1487–1502.

[8]Iess, L., Tortora, P., Anderson, J. D., Asmar, S. W., Barbinis, E., Bertotti, B., Fleischman, D. U., Gatti, M. S., Goltz, G. L., Herrera, R. G., Lau, E., and Oudrhiri, K., "The Cassini Solar Conjunction Experiment: A New Test for General Relativity," *Aerospace Conference Proceedings*, Vol. 1, Inst. of Electrical and Electronics Engineers, Piscataway, NJ, March 2003, pp. 205–211.

[9]Abbate, S. F., Armstrong, J. W., Asmar, S. W., Barbinis, E., Bertotti, B., Fleischman, D. U., Gatti, M. S., Goltz, G. L., Herrera, R. G., Iess, L., Lee, K. J., Ray, T. L., Tinto, M., Tortora, P., and Wahlquist, H. D., "The Cassini Gravitational Waves Experiment," *Gravitational-Wave Detection*, SPIE—The International Society for Optical Engineering, Bellingham, WA, 2003, pp. 90–97.

[10]Bertotti, B., Comoretto, G., and Iess, L., "Doppler Tracking of Spacecraft with Multifrequency Links," *Astronomy and Astrophysics*, Vol. 269, Nos. 1–2, 1993, pp. 608–616.

[11]Tortora, P., Iess, L., and Ekelund, J. E., "Accurate Navigation of Deep Space Probes Using Multifrequency Links: The Cassini Breakthrough During Solar Conjunction Experiments," *Proceedings of the World Space Congress*, AIAA, Reston, VA, 2002.

[12]Tortora, P., Iess, L., and Herrera, R. G., "The Cassini Multifrequency Link Performance During 2002 Solar Conjunction," *Aerospace Conference*

Proceedings, Vol. 3, Inst. of Electrical and Electronics Engineers, Piscataway, NJ, 2003, pp. 1465–1473.

[13]Resch, G. M., Keihm, S. J., Lanyi, G. E., Linfield, R. P., Naudet, C. J., Riley, A. L., Rosenberger, H. W., and Tanner, A. B., "The Media Calibration System for Cassini Radio Science: Part III," The Interplanetary Network Progress Rept. 42-148, Jet Propulsion Lab., California Inst. of Technology, Pasadena, CA, Feb. 2002, pp. 1–12.

[14]Keihm, S. J., "Water Vapor Radiometer Measurements of the Tropospheric Delay Fluctuations at Goldstone over a Full Year," The Telecommunications and Data Acquisition Progress Rept. 42-122, Jet Propulsion Lab., California Inst. of Technology, Pasadena, CA, Aug. 1995, pp. 1–11.

[15]Weeks, C., Miller, J. K., and Williams, B., "Calibration of Radiometric Data for Relativity and Solar Plasma During a Solar Conjunction," *Journal of the Astronautical Sciences*, Vol. 49, No. 4, 2001, pp. 615–628.

[16]Moyer, T. D., "Formulation for Observed and Computed Values of Deep Space Network Data Types for Navigation," Deep-Space Communications and Navigation Series, Jet Propulsion Lab., JPL Publ. 00-7, California Inst. of Technology, Pasadena, CA, Oct. 2000.